Self-associating behavior of acetone in liquid krypton

The Self-Associating Behavior of Acetone in Liquid Krypton

Liene I. De Beuckeleer, Wouter A. Herrebout*

Department of Chemistry, University of Antwerp, Groenenborgerlaan 171, 2020 Antwerp, Belgium

Abstract

Acetone molecules are inclined to self-associate through dipole-dipole interactions because of their large dipole moment. Infrared spectroscopy of compounds dissolved in liquid noble gases supported by high level a*b initio* calculations allows investigating the self-associating behavior and determining the thermodynamical properties. In this study, infrared spectra of various concentrations of acetone dissolved in liquid krypton are recorded at constant temperature. Overlapping monomer and dimer spectra are separated by analyzing the obtained datasets with numerical methods based on least-squares fitting. Although acetone is known to self-associate, only a few spectral features have been presented in literature before. In this study, the application of new numerical approaches succeeds in resolving overlapping spectra and allows observing isolated acetone dimer absorption bands for the complete mid infrared spectrum. Using datasets of spectra recorded at temperatures between 134 and 142 K, the experimental standard dimerization enthalpy was determined to be -10.8 kJ mol^{-1}. MP2/aug-cc-pVDZ calculations predicted a stacked and planar dimer geometry of which the stacked geometry is more stable. Combining MP2 energies and single point corrections involving CCSD(T) calculations and Complete Basis Set extrapolations based on the MP2/aug-cc-pVDZ equilibrium geometry lead to complexation energy of -28.4 kJ mol^{-1} for the stacked geometry and -15.1 kJ mol^{-1} for the planar

geometry. The corresponding values for the complexation enthalpies in solution, obtained by combining these values with corrections for thermal and solvent influences are -13.7 and -5.8 kJ mol^{-1}.

1. INTRODUCTION

Because of their large dipole moment[1], acetone molecules are inclined to interact with each other through long range dipole-dipole interactions and short-range C-H···O hydrogen bonding interactions. As a result, the properties of acetone dimers have been the subject of various studies. Early evidence for the self-association of acetone and other ketones was reported by T.F. Lin and co-workers.[2] These authors investigated the self-association of acetone, 2,3-butanedione and acetylacetone in carbon tetrachloride and hexadecane solutions by partition, solubility and isopiestic techniques, and estimated the equilibrium constants for the dimerization reaction at 15 and 25°C. The complexation enthalpy for dimerization of acetone in hexadecane was derived to be -11.7 kJ mol^{-1}. Additional evidence supporting the idea of self-association of acetone in the liquid and in the vapor phase was reported by D.J. Frurip *et al*.[3] These authors measured the thermal conductivity of acetone vapor at temperatures between 341 and 378 K over the pressure range of 200-1200 Torr, and estimated the standard enthalpy for acetone dimer formation to be -13.5 ± 1.4 kJ mol^{-1}. The authors supported their experimental studies with *ab initio* molecular orbital calculations, and concluded that the dimer had a cyclic structure stabilized by two C-H···O hydrogen bonds.

Early spectroscopic evidence for acetone self-association was reported by B. Tiffon *et al.*[4], W. Schindler *et al*.[5] and E. Knözinger *et al*.[6] The first authors studied ^{17}O NMR chemical shifts and linewidths at variable temperature. The chemical shift data were found to be consistent with a monomer-dimer equilibrium with a standard association enthalpy and entropy of -4.6 kJ mol^{-1} and -35.6 J mol^{-1} K^{-1}. Analysis of the linewidth measurements suggested that the dimer does not reorient in the liquid as a rigid unit, but must rather be considered as a short-lived electrostatic-collided complex. W. Schindler and co-workers used Raman spectroscopy to study the effect of pressure on the C=O stretching wavenumber and the isotropic line shape of this mode in liquid acetone.[5] E. Knözinger *et al*. focused on the far-infrared spectra of acetone trapped in argon matrices, and concentrated on the changes observed while annealing the matrices.[6] More recent spectroscopic studies on acetone self-association involve, amongst others, the combination of

molecular beam experiments with photoionization detection with tunable coherent vacuum-ultraviolet spectroscopy[7-8] and near edge-X-ray absorption spectroscopy [9].

Continuing on experimental studies by M.R. Jalilian[10] describing the infrared and NMR spectra of binary azeotropes formed by mixing acetone and cyclohexane, G. Arivazhagan *et al*.[11] recently reported on a combined experimental and theoretical study on the behavior of acetone in cyclohexane solutions. The spectroscopic studies were performed using traditional FTIR, ^{13}C NMR and UV-vis spectroscopic methods and mainly focused on changes in wavenumbers and chemical shifts observed when passing from the pure liquids to a binary solution. Amongst other changes, blue shifts observed for the C=O stretching mode, the C–C=O bending modes and the C–H stretching modes were explained as the result of molecular complexes. From the limited data available it was concluded that in its pure form, acetone exists as molecular entities self-associated through blue-shifting C–H···O hydrogen bonds, while in the mixture with cyclohexane the dimers are dissociated so that only monomers remain.

It must be noted explicitly that in the latter studies, evidence for the occurrence of acetone dimers in solutions was derived from changes in wavenumbers or chemical shifts, and that for none of the solutions studied, separate bands due to monomers and complexes were reported. This observation is in line with the earlier observations suggesting that in the liquid phase, interactions between acetone molecules mainly give rise to short-lived species formed during the collision of two molecules. Taking into account that individual spectral features proving the simultaneous occurrence of monomers and binary complexes have been observed for a variety of complexes involving acetone as a Lewis base, and considering that these complexes often had a complexation enthalpy similar to or even smaller[12-13] than the numbers reported above for the acetone dimers, however, there seems no reason why such features should not be present for acetone dimers. We therefore believe that the observations and the conclusions derived from the above studies should be questioned.

Building on experimental evidence showing the applicability to characterize homo and heterodimers[14-19], infrared spectroscopy of solutions in liquefied noble gases can shed light on the nature of acetone dimers and, eventually, also higher associations. The advantage of the approach is based on the fact that the inert gases used as a solvent create a weakly interacting environment that, combined with the low temperatures used, lead to small bandwidths and thus

facilitates the detection of complex bands only slightly shifted from the monomer modes. In addition, the cryosolutions can be used to determine thermodynamical properties of the species studied as the solutions are in chemical equilibrium. Therefore, cryospectroscopy also allows the determination of the standard enthalpy of formation in an independent way, of which the resulting values can be used to assess the scattered literature data summarized above.

For heterodimers, analysis of the spectra obtained for mixed cryosolutions typically involves subtraction procedures in which the spectra of the monomers and of the complexes are separated by recording monomer spectra at exactly the same temperature, and by rescaling and subtracting these spectra from those obtained for the mixed solution. Similar to gas-phase studies including amongst others hydrogen bonded complexes with dimethylamine[20] and halothane[21-23], the rescaled monomer spectra represent the contributions of the respective monomers studied, while the difference spectra obtained show the spectral features due to the complexes present. For studies involving homodimers, including the case of acetone dimer studied here, subtraction based procedures often are hampered by the fact that even for lowest concentrations studied spectra typically contains spectral features due to monomers and homodimers. Hence, for such systems, no monomer only spectra required for reliable subtraction processes are available. To overcome the limitations of the subtraction procedures, we have recently reported on more sophisticated approaches based on constrained least-squares fitting algorithms.

To be able to rationalize the spectral features related to the weak molecular complexes formed between acetone molecules, in this study, infrared spectra of solutions in liquid krypton (LKr) containing mole fractions of acetone varying between 4.2×10^{-4} and 5.6×10^{-5} are recorded, at temperatures between 134 and 142 K. The resulting spectra are analyzed using a least-squares fitting based method similar to that used for the studies of HCl and pyrrole oligomers.[17-18] The spectroscopic studies are supported by MP2 and single point CCSD(T) *ab initio* calculations to predict the structural, energetical and spectroscopic properties of the different complexes that can be formed, and by Monte Carlo Free Energy Perturbation (MC-FEP) and statistical thermodynamical calculations to rationalize the effects of temperature and of solvatation on the complexation enthalpies measured. The results show that, in contrast to earlier studies, separate bands due to acetone monomer and acetone dimer can be identified. Analysis of the temperature dependence also allows the complexation enthalpy for the dimer in cryosolutions and in the gas phase to be reliably determined. The results for the first time show that cryosolutions can yield

interesting information on complexes largely determined by long-range dipole-dipole interactions and that applications should thus not be limited to typical Lewis base - Lewis acid interactions involving, amongst others, hydrogen and boron halides, C–H hydrogen and C–X halogen bond donors and electron deficient molecules such as CO_2, OCS and N_2O.[15,24-25]

2. EXPERIMENTAL DETAILS

The sample of acetone ($(CH_3)_2CO$, 99,5%) was purchased from Acros and was used without further purification. The krypton used as a cryosolvent had a stated purity of 99.9995% and was supplied by Air Liquide.

Infrared spectra of acetone in LKr were recorded on a Bruker IFS 66v Fourier transform spectrometer. A Globar source was used in combination with a Ge/KBr beamsplitter and a LN_2-cooled broad band MCT detector. All interferograms were averaged over 500 scans, Blackman-Harris 3-term apodized and Fourier transformed with a zero filling factor of 4 to yield spectra with a resolution of 0.5 cm^{-1}. The experimental set-ups used to investigate the solutions in liquid noble gases have been described before.[26] In the actual cryostat, a liquid cell with 1 cm path length and equipped with wedged Si windows was mounted below a LN_2 Dewar. The temperature of the cell body is measured using a Pt-100 thermoresistor. The SunRod electric minicartridge heater is controlled using a Eurotherm 3504 PID controller. The temperature of the solutions were stabilized at 134, 135, 136, 137, 138, 139, 140, 141 or 142 K, the temperature variation during a typical run being less than 0.05 K. Spectra were obtained and pre-analyzed using OPUS 6.5. The data sets consisted of 117 to 153 spectra. Further calculations were performed using Matlab.[27]

The mole fractions of acetone used for the data sets are difficult to accurately quantify[28-29], but are estimated to vary between 4.2×10^{-4} and 5.6×10^{-5}. As acetone has a limited solubility in LKr[12-13,30-31], the amount of acetone dissolved in the cryosolvent was increased by increasing the temperature to 160 K after filling the cell at 123 K and then lowering it back to the wanted temperature. The concentrations used are chosen so that the region between minimum and maximum absorbance is uniformly covered and all measured regions have absorbances below 1. Figure 2 shows five spectra of the data set of 138 K for the relevant regions of the spectrum.

As the outcome of the used fitting procedures are perturbed by baseline artifacts, baseline corrections on the complete data set were performed using spectra of pure LKr recorded under exactly the same conditions. Another critical parameter often hampering the numerical analyses to be performed is related to small traces of solid, amorphous or crystalline, water suspended in the solution or condensed onto the cold elements present in the cryostat and/or detector. The traces are observed to slightly increase during experiment, and, due to changes in relative intensities, are difficult to subtract. To account for remaining baseline drifts, which we believe are due to small temperature changes inside the spectrometer due to the colder parts present, an additional straight line baseline correction was applied to all data. These lines are drawn connecting points where the absorbance is known to be zero. In the case of acetone these straight lines were generated from 3752 to 3057, from 3057 to 2876, from 2876 to 2812, from 2812 to 2667, from 2667 to 1935, from 1935 to 1615, from 1615 to 1286, from 1286 to 1140, and from 1140 to 960 cm^{-1}.

3. COMPUTATIONAL DETAILS

To support our experimental measurements, geometries and harmonic vibrational frequencies were obtained from *ab initio* MP2 calculations performed using Dunning's augmented correlation consistent basis set of double zeta quality (aug-cc-pVDZ) in Gaussian09.[32] The geometry optimizations were performed using default optimization settings. The counterpoise technique as proposed by Boys and Bernardi was used during all *ab initio* calculations to account for basis set superposition error.[33] More reliable energies at the basis set limit were calculated with Molpro[34] using the extrapolation scheme of Truhlar, in which the effect of electron correlation is obtained from MP2 calculations[35].

$$E_{CBS}^{HF} = \frac{3^{\alpha}}{3^{\alpha} - 2^{\alpha}} E_3^{HF} - \frac{2^{\alpha}}{3^{\alpha} - 2^{\alpha}} E_2^{HF} \quad (1)$$

$$E_{CBS}^{cor,MP2} = \frac{3^{\beta}}{3^{\beta} - 2^{\beta}} E_3^{cor,MP2} - \frac{2^{\beta}}{3^{\beta} - 2^{\beta}} E_2^{cor,MP2} \quad (2)$$

In these calculations α = 3.4 and β=2.2,[35] while energies with subscript 2 and 3 are calculated using the aug-cc-pVDZ and aug-cc-pVTZ basis sets respectively.

Furthermore, a correction for higher degree correlation effects is made using Hobza's method,[36-37] yielding results of $E_{CBS}^{CCSD(T)}$ quality.

$$\Delta E^{CCSD(T)} = \left| E^{CCSD(T)} - E^{MP2} \right|_{aug-cc-pVDZ} \quad (3)$$

$$E_{CBS}^{CCSD(T)} = E_{CBS}^{HF} + E_{CBS}^{cor,MP2} + \Delta E^{CCSD(T)} \quad (4)$$

A calculated complexation energy ΔE(CCSD(T)) is transformed into vapor phase complexation enthalpy ΔH°(vap,calc), by accounting for thermal and zero-point vibrational contributions. Correction of this calculated enthalpy value with solvent effects yields a complexation enthalpy in solution ΔH°(LKr,calc) which can be compared with the experimental complexation enthalpy ΔH°(LKr). Corrections for thermal effects and zero-point vibrational contributions were obtained using statistical thermodynamics [38], whereas the effects of solvation were accounted for using the Monte Carlo Free Energy Perturbation (MC-FEP) approach in an in-house modified version of BOSS 4.0.[39]

4. RESULTS AND DISCUSSION

4.1 Vibrational modes of acetone monomer

For molecules with C_{2v} symmetry, x- and y-axes are often interchanged and numbering of the vibrational modes often leads to confusion.[40] The definitions of the axes and used in this study and the numbering of the vibrational modes is given in the supporting information.

Figure 1 shows the spectrum of the recorded data set with the highest concentration of acetone dissolved in LKr at 138 K. The mid infrared vibrational spectrum is characterized by an intense absorption band assigned to the carbonyl stretching vibration, ν_3, around 1725 cm^{-1}. This band has been one of the most popular features to study the clustering interactions involving acetone.[5,8,41-43] Other signals that have been used involve the C–H stretches[7-8] near the 3009-2926 cm^{-1} region, the CH_3 deformation modes ν_{21} and ν_5 near 1361-1355 cm^{-1}, and the asymmetric C–C stretching, ν_{22} near 1217 cm^{-1} [43]. In the next paragraphs we will report on the self-associating behavior of acetone by studying the effect of varying the concentration in all spectral regions, i.e. in the region often used to study hetero complexes and in the neglected regions.

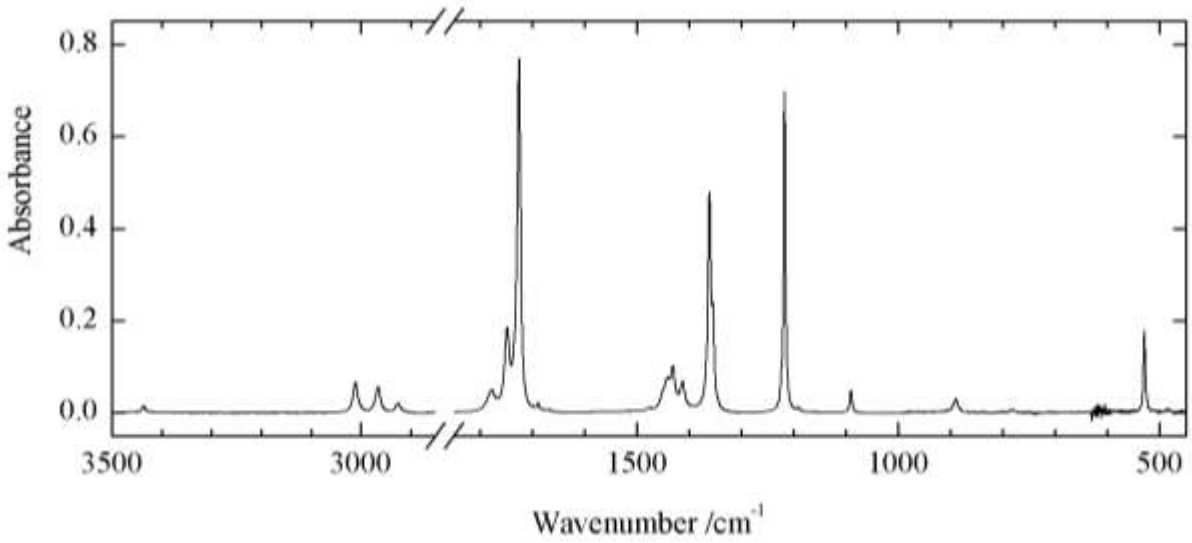

Figure 1. Infrared spectrum of acetone dissolved LKr recorded at 138 K

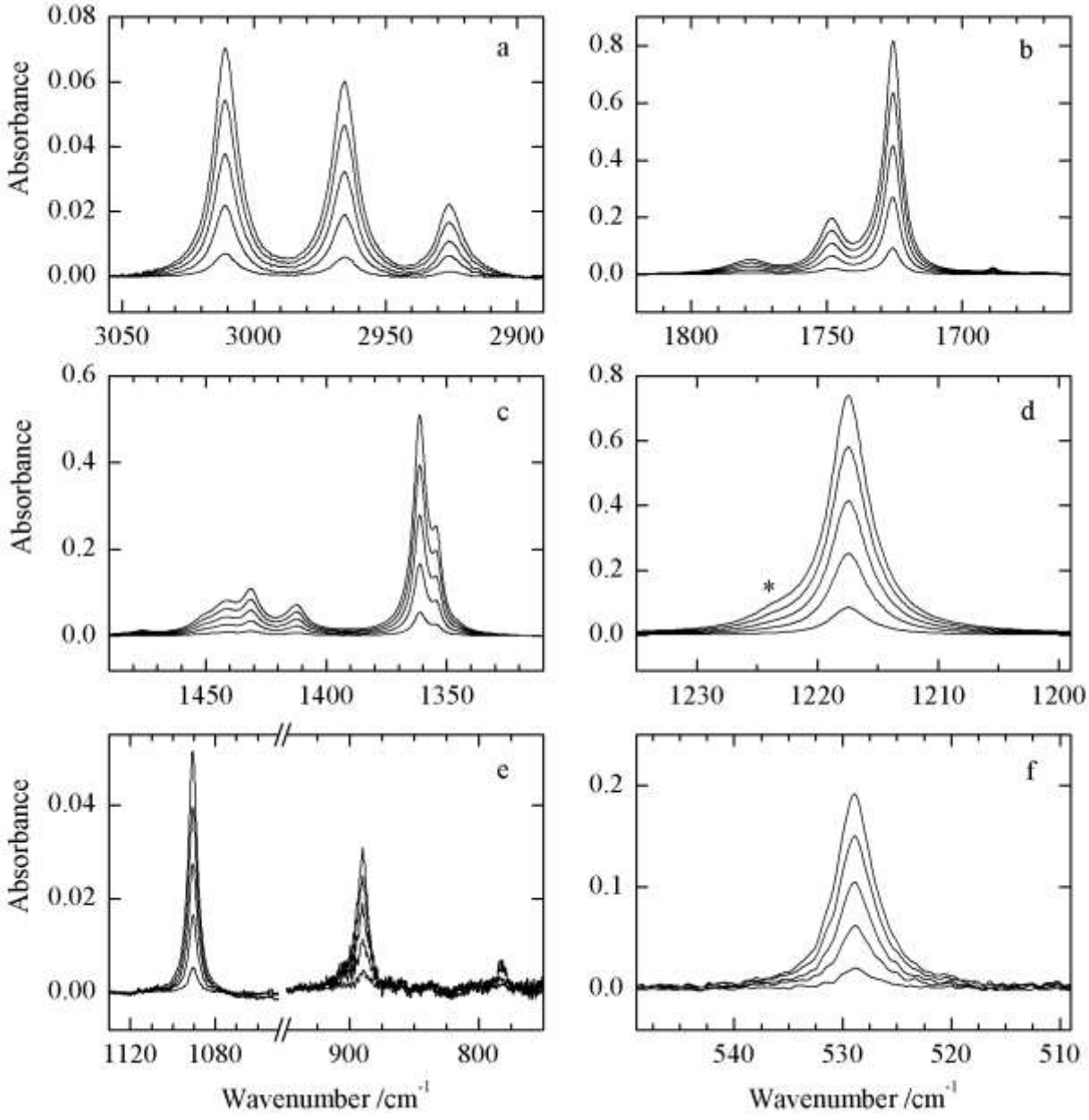

Figure 2. Infrared spectra of solutions of acetone in LKr, at 138 K. The spectra shown for each of the species represent only a small fraction of the spectral database used in the fitting procedures. * Indicates a new absorption band emerging when increasing the acetone concentration.

4.2 Least-squares fitting of quadratic polynomials

When self-association occurs, an increase in concentration should yield new bands, due to oligomers, becoming noticeable in the spectra. Figure 2 shows the dependence with the concentration of the acetone cryosolutions of the most relevant spectral regions, illustrated with a selection of 5 spectra from the 138 K data set. New visual features arising with increasing concentration except for one new band, indicated with * in panel 3d, appearing as a shoulder to the ν_{22} transition.

To determine if other dimer features are present in the remaining spectral regions, the data set was analyzed using the newly developed least-square based approach, with the purpose of isolating overlapping absorption bands of monomeric and oligomeric species. It has already been validated with the self-associating molecules HCl and pyrrole.[17-18]

The general concept of the method used is based on the fact that, with some exceptions[44-45], cryosolutions are known to be in thermodynamical equilibrium. The spectra for cryosolutions of self-associating species therefore are a superposition of monomer spectra and spectra of the different complexes, with the relative absorbances determined by the equilibrium concentrations C and the molar attenuation coefficients ε of the monomeric species and of the associations formed. The latter are determined by the equilibrium constant K involved.

$$2\ \text{monomer} \rightleftharpoons \text{dimer} \qquad K_2 = \frac{C_{dimer}}{C_{monomer}{}^2} = \frac{C_{di}}{C_{mono}{}^2} \tag{5}$$

Starting from these assumptions, for each arbitrary wavenumber $\tilde{\nu}_i$ the measured absorbance A_{exp} can be written as a sum of absorbance contributions related to the monomer A_{mono} or to one of the oligomers, in this case only dimer A_{di}, i.e.

$$A_{exp}(\tilde{\nu}_i) = A_{mono}(\tilde{\nu}_i) + A_{di}(\tilde{\nu}_i) \tag{6}$$

By choosing an appropriate wavenumber $\tilde{\nu}_m$ for which the absorbance is due to monomer only, i.e.

$$A_{exp}(\tilde{\nu}_m) = A_{mono}(\tilde{\nu}_m) \tag{7}$$
$$\text{and } A_{di}(\tilde{\nu}_m) = 0$$

and by using Lambert-Beer's law

$$A_j(\tilde{\nu}_i) = \varepsilon_j(\tilde{\nu}_i) C_j d \tag{8}$$

with ε as the molar attenuation coefficient, C as the concentration in the solution, j as the type of species and d as the path length of the cell used, the different contributions in eq.6 can be rewritten in terms of the absorbance of the monomer wavenumber $\tilde{\nu}_m$;

$$A_{mono}(\tilde{\nu}_i) = a_1(\tilde{\nu}_i, \tilde{\nu}_m) A_{mono}(\tilde{\nu}_m) \tag{9}$$

$$A_{di}(\tilde{\nu}_i) = a_2(\tilde{\nu}_i, \tilde{\nu}_m) A_{mono}(\tilde{\nu}_m)^2 \tag{10}$$

The coefficients $a_{\mathrm{p}}(\tilde{\nu}_i, \tilde{\nu}_m)$,with p representing the polynomial degree, used in these expressions are defined as

$$a_1(\tilde{\nu}_i, \tilde{\nu}_m) = \frac{A_{mono}(\tilde{\nu}_i)}{A_{mono}(\tilde{\nu}_m)} = \frac{\varepsilon_{mono}(\tilde{\nu}_i)}{\varepsilon_{mono}(\tilde{\nu}_m)} \tag{11}$$

$$a_2(\tilde{\nu}_i, \tilde{\nu}_m) = \frac{A_{di}(\tilde{\nu}_i)}{A_{mono}(\tilde{\nu}_m)^2} = a_1(\tilde{\nu}_i, \tilde{\nu}_m)^2 \frac{\varepsilon_{di}(\tilde{\nu}_i)}{\varepsilon_{mono}(\tilde{\nu}_m)^2} \frac{1}{d} K_2 \tag{12}$$

Substituting the eq. 9 and 10 in eq. 6 results in

$$A_{exp}(\tilde{\nu}_i) = a_1(\tilde{\nu}_i, \tilde{\nu}_m) A_{mono}(\tilde{\nu}_m) + a_2(\tilde{\nu}_i, \tilde{\nu}_m) A_{mono}(\tilde{\nu}_m)^2 \tag{13}$$

The above equation shows that for any arbitrary wavenumber $\tilde{\nu}_i$, the contributions due to the different species present can in principle be derived by plotting, for all solutions and concentrations studied, the measured absorbances at $\tilde{\nu}_i$ versus the corresponding monomer absorbances measured at the given reference wavenumber $\tilde{\nu}_m$, and using least-squares to fit a polynomial to the resulting data. Examples of typical fits are presented in Figure 3.

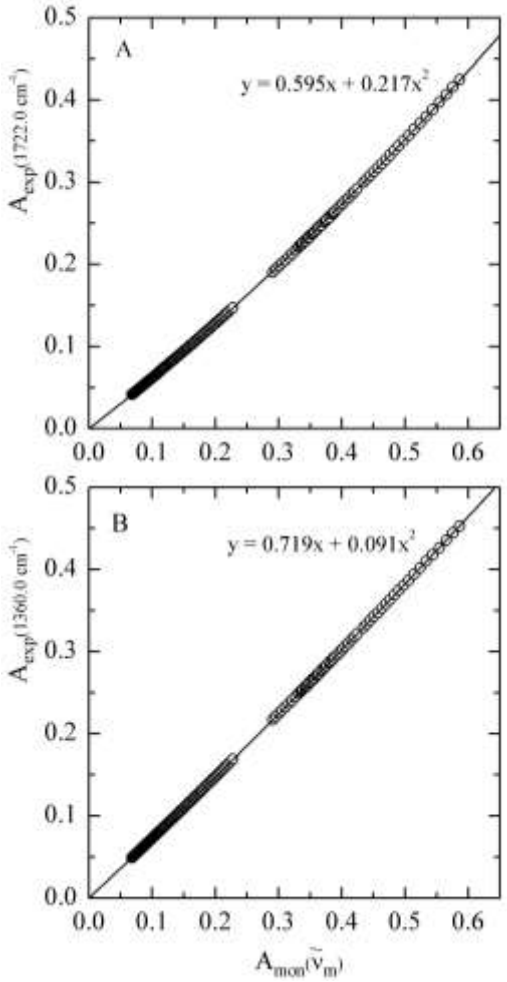

Figure 3. Two examples of a quadratic polynomial fitted through the measured absorbances for different concentrations at a certain wavenumber versus the monomer absorbances for different concentrations at the reference wavenumber $\tilde{\nu}_m$ set at 1216.5 cm^{-1}. Panel A illustrates the fit for the absorbances measured at 1722.0 $cm^{-1;}$ Panel B gives the data for 1360.0 cm^{-1}.

The chosen reference wavenumber $\tilde{\nu}_m$ is used as an internal standard and is chosen based on the fact that no features due to self-association are observed or expected to appear in the region considered. In the case of acetone, $\tilde{\nu}_m$ was chosen in the spectral region of the ν_{22} transition. As described before this band shows a dimer feature blue shifted from the monomer band center, for this reason the absorbance at a wavenumber on the lower wavenumber side is more likely to only have a monomer contribution. $\tilde{\nu}_m$ was set to be 1216.5 cm^{-1}. In order to check if the choice of this wavenumber is suitable we compare the results of the analysis with the outcome of a subtraction routine. In the case of the self-associating species the subtraction routine can be performed by scaling a low concentration spectrum to a high concentration spectrum, resulting in

a spectrum that contains only signals of oligomeric species. As observed in the earlier HCl study [18], low concentration spectra often already contain traces of oligomers, leading to an underestimation of the presence of the oligomers in the oligomers spectrum. The results obtained using subtraction procedures therefore must always be treated with caution. Although a subtraction routine underestimates the presence of the dimer and in principle cannot be used for quantitative measurements, it can still be used to give us an idea of the shape and width of the dimer band. The dimer contribution resulting from the subtraction routine is illustrated with the red trace in Figure 4.

Figure 4a1 and a2 shows the monomer and dimer contribution, for the cryosolution containing an approximate mole fraction of 4.2 x 10^{-4} and recorded at 138 K. The results shown are derived by analyzing the data set using the 2nd degree polynomial as described in equation 13. In Figure 4a2 it can be seen that the dimer contribution at $\tilde{\nu}_m$, at 1216.5 cm^{-1}, is zero. This result is determined by the general assumption suggesting that for all solutions studied, the measured absorbance at the reference wavenumber is solely determined by monomer species. Comparing the results in Figure 4a2 with the dimer contribution derived from an approximate subtraction procedure, illustrated with the red trace, it is obvious that this assumption is not completely valid. Indeed, the absorbance at 1216.5 cm^{-1} should not be zero but should be approximately 0.02.

The conclusion that the absorbance at $\tilde{\nu}_m$, $A_{exp}(\tilde{\nu}_m)$, not only consists of a monomer contribution, but actually consists of a monomer and dimer contribution, $A_{mono}(\tilde{\nu}_m)$ and $A_{di}(\tilde{\nu}_m)$, somewhat weakens the choice for the reference wavenumber made. However, as all other modes are expected to show similar dimer bands largely or completely overlapping with the monomer bands, apart from data in the immediate vicinity of 1216.5 cm^{-1}, no other options for reliable reference wavenumbers are available. To overcome the problem, a somewhat arbitrary correction was introduced, in which the value of $A_{mono}(\tilde{\nu}_m)$ was corrected by i) estimating the dimer contribution and ii) subtracting this value from $A_{exp}(\tilde{\nu}_m)$.

$$A_{mono}(\tilde{\nu}_m) \approx A_{exp}(\tilde{\nu}_m) - A_{di}(\tilde{\nu}_m) \qquad (14)$$

To estimate the value of the dimer contribution, the band derived from the fitting procedure was symmetrized over an axis of symmetry originating from the maximum of the band. The axis of symmetry chosen is indicated with the dash dot line in panel 4b. The $A_{mono}(\tilde{\nu}_m)$ values obtained

by correcting the absorbance of the symmetrized dimer band at $\tilde{\nu}_m$ from $A_{exp}(\tilde{\nu}_m)$ leads to the results shown in Figure 4b.

Comparison of data in Figure 4b show that, although the agreement is already significantly improved, the resulting dimer band obtained by using the corrected monomer intensities, and that obtained from the approximate subtraction is far from excellent. Realizing that the monomer intensities required for the determination of the dimer band are directly influenced by the outcome, i.e the dimer contribution itself, we attempted to improve the agreement using a self-consistent procedure, in which the correction is repeated until only minor changes in the calculated spectra of monomer and dimer are observed. In order to improve the resemblance of fitted dimer band with the subtracted one, it was chosen to shift the axis of symmetry for 1.5 cm^{-1} to the lower wavenumber side, as illustrated in Figure 4c. This resulted in a larger correction for $A_{exp}(\tilde{\nu}_m)$ indicated with the arrow in Figure 4c. As the fitted result indeed showed more resemblance with the subtraction it was decided to use this method to analyze vibrational spectrum of acetone. Also in this case multiple iterations were introduced, but again no major changes of the dimer contributions were observed. The result shows that also for the other modes, spectral features illustrating self-association can be identified. As these features typically escape detection in classical subtraction procedures or visual comparisons, the results therefore clearly illustrate the added value of the least-squares based method.

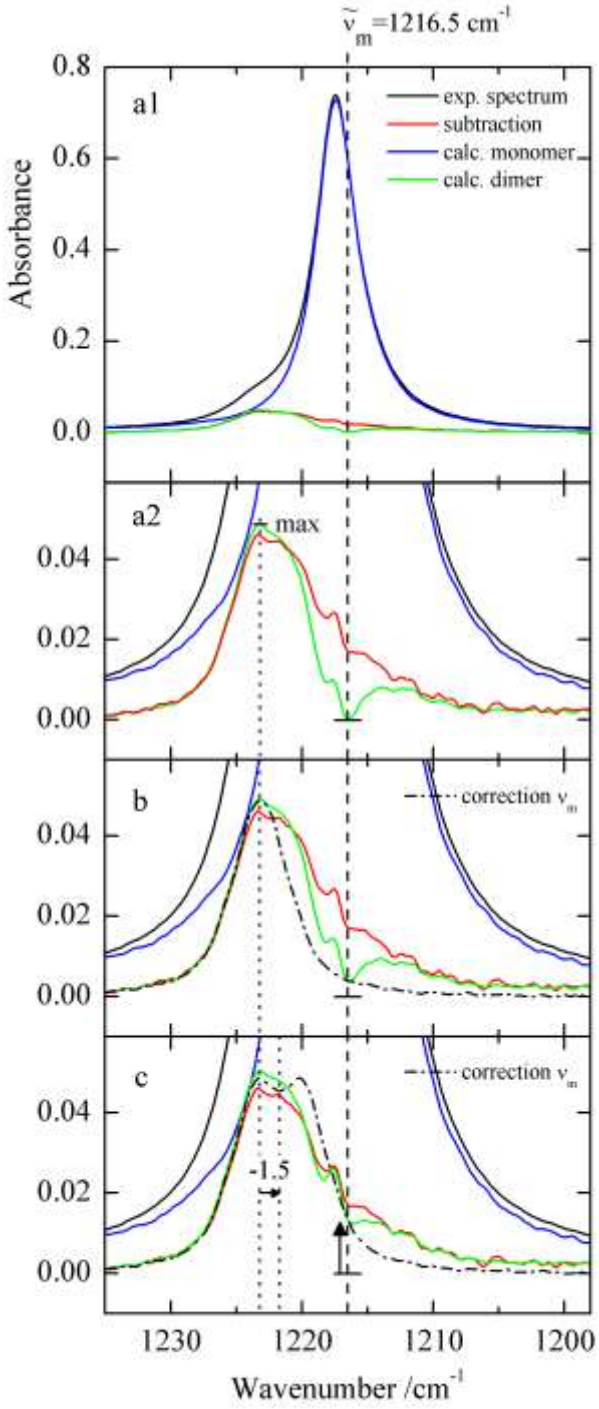

Figure 4. Results from least-squares procedures using a 2nd degree polynomial. The monomer wavenumber at 1216.5 cm^{-1} is indicated with the vertical dashed line. The upper panel shows the calculated monomer and dimer contributions without corrections of $\tilde{\nu}_m$ with a blue and green trace. The red trace illustrates the dimer contribution obtained from a subtraction procedure. In panel a2 the dimer contribution is magnified. The absorbance at $\tilde{\nu}_m$ is corrected by reflecting the higher wavenumber half of the calculated dimer band at the

wavenumber with maximum absorbance indicated with the dotted line. This correction and the resulting monomer and dimer contributions of the first iteration are shown in panel b with a dash dot trace. In order to get a better resemblance with the subtraction trace the axis of symmetry was moved for 1.5 cm^{-1} to the lower wavenumber side. The new correction and the results of the first iteration using this correction are shown in panel c.

4.3 Vibrational spectra of the acetone monomer and dimer

By using the corrected monomer intensity obtained for the reference wavenumber 1216.5 cm^{-1}, reliable data can also be derived for the other spectral regions for which, at first sight, no dimer contributions are to be expected. Figure 5 shows the fitted monomer and dimer contributions for the most important regions of the acetone spectrum applying the method illustrated in Figure 4c to the data set of 138 K. The results show that apart from the dimer band at 1222.7 cm^{-1} other dimer features can be reliably predicted, at wavenumbers close to or almost identical to those of the monomer species. The assignment of the experimental spectra is presented in Table 1. The approximate description of vibrational modes adopted is similar to those previously used by Dellepiane *et al*.[46] and Consani *et al*.[41] The assignments of the monomer closely follow those reported for the compound in the gaseous phase[46] and in the solid argon matrix[41-42]. For the dimer, only few results are available in previous literature studies and these will be mentioned further down the text.

In the C–H stretching region (Figure 5a), three main monomer bands assigned to respectively the degenerate stretches, ν_1 and ν_{18}, the stretch ν_{13} and the degenerate stretches, ν_2 and ν_{19} are observed at 3011.1, 2965.7 and 2926.1 cm^{-1}. For these monomer bands, dimer features shifted by -2.0, 0.0 and 0.1 cm^{-1} respectively, are predicted at 3009.1, 2965.7 and 2926.2 cm^{-1}. These values differ from the gas phase IR/VUV spectroscopy values reported by Guan *et al*.[8] who reported red and blue shifts of -8, 4 and 0 cm^{-1} respectively. The reason for the discrepancies is not fully understood but most probably is related to solute-solvent interactions in the cryosolutions slightly perturbing both the fundamental wavenumbers of the modes present and the Fermi resonances with overtones and combinations bands present. It is interesting to note that the C–H stretching region was also studied by Matsuda *et al*.[7] The data reported by these authors were also based on the combination of infrared spectroscopy and VUV photoionization detection, but did not lead to any observation of dimer bands in this region.

Although perturbed by Fermi resonance involving the $\nu_{22} + \nu_{24}$ transition[47-48], the intense C=O stretching mode has been the most popular transition to study the intermolecular interactions with acetone.[8,41-43] The results of the fitting procedures of this spectral region are displayed in Figure 5b. The monomer band in LKr was found to appear near 1725.6 cm^{-1}. The fitting procedure revealed a dimer band, slightly redshifted from the monomer by -2.2 cm^{-1}, at 1723.4 cm^{-1}. Combination of the small shift observed and the strong infrared intensity observed for the monomer, most probably, is the reason why no comparable dimer signal has been reported in literature before.

In the 1500-1300 cm^{-1} spectral region (Figure 5c), the monomer gives rise to five fundamental transitions due to CH_3 deformation modes: the weaker bands due to ν_{14}, ν_4, ν_{20} appear at 1451.0, 1431.3 and 1412.3. The more intense modes ν_{21}, ν_5 modes are observed at, 1361.1 and 1354.6 cm^{-1}. Apart from these bands, in the spectra of the cryosolutions, additional bands related to dimer formation are observed for every mode, except for ν_{14}. These dimer signals all show complete overlap with the monomer bands and escaped detection in earlier studies.

Panel 5d shows the results for the C–C asymmetric stretching region discussed in detail above. The dimer band at 1222.7 cm^{-1} is blue shifted from the monomer at 1217.4 cm^{-1}. The shift of 5.3 cm^{-1} is the largest observed complexation shift in the recent experimental study. No spectral features related to this band have been reported before.

Panels Figures 5e and 5f illustrates the appearance of complex bands for four much weaker fundamentals. The monomer bands at 1090.2 and 530.2 cm^{-1} are assigned to the out-of-plane CH_3 rock and the C=O in-plane bending vibration, and are accompanied by a dimer signal emerging 2.0 and 1.3 cm^{-1} blue shifted from the monomer, respectively. The presence of traces of solid water in the solution perturbs the analysis in the 1000-700 cm^{-1} region and limits the signal-to-noise. Consequently, a reliable analysis of the features in this region due to the in-plane CH_3 rocking and the symmetric C–C stretching modes at ~889 and ~782 cm^{-1} is not possible.

The weak feature at ~893 cm^{-1} can tentatively be assigned to the dimer. Due to the limited signal-to-noise ratio, we decided to remain cautious about its nature and to not include this feature in the list of observed wavenumbers. The predictions for the ~782 cm^{-1} band suggests an unrealistically compensation effect in which the monomer spectrum is largely overestimated and is compensated by a negative dimer contribution. This band, again, is not included in Table 1.

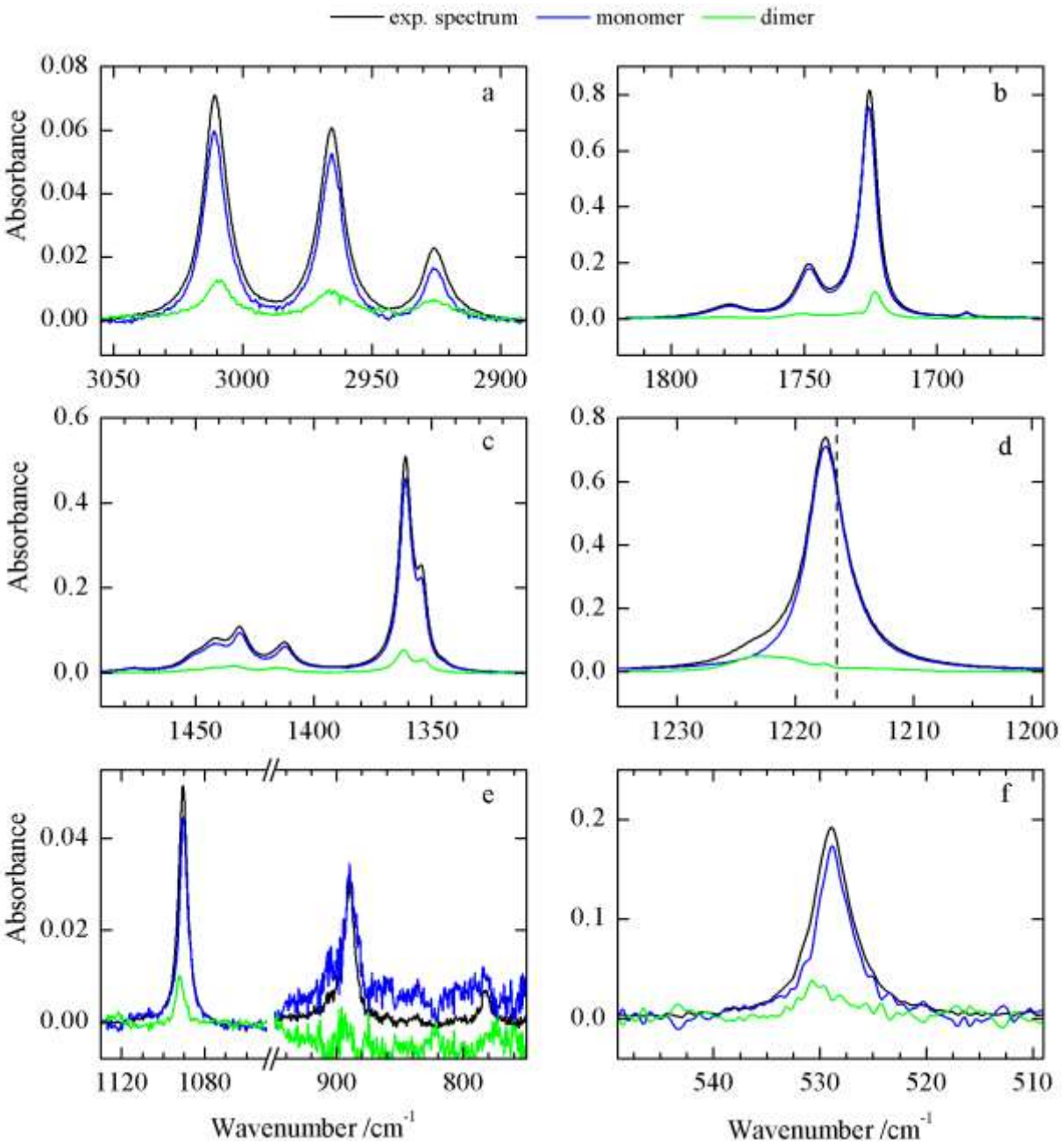

Figure 5. Results from least-squares procedures using a 2nd degree polynomial with a corrected absorbance at the monomer wavenumber at 1216.5 cm^{-1} (dashed line in panel d).

Table 1 Assignment of experimental monomer and dimer absorption bands of acetone in solution with krypton at 138 K and a comparison with previous literature investigations [a]

Monomer						Dimer			
			experimental			experimental		calculated MP2/aug-cc-pVDZ	
Number	approximate description [c] [41,49]	symm	gas phase[46]	solid Ar matrix 9 K [41-42]	liquid Kr 138 K	liquid Kr 138 K	$\Delta\nu$	stacked $\Delta\nu$	planar $\Delta\nu$
$2\nu_3$		A_1	3453		3436.7				
ν_1	νC–H $_{as}$	A_1	3018.5	3018.6	3011.1	3009.1	-2.0	-5.7	-2.7
ν_{18}	νC–H $_{as}$	B_2						-5.6	-5.3
ν_{13}	νC–H	B_1	2972	2972.6	2965.7	2965.7	0.0	3.0	-1.5
ν_2	νC–H $_{sym}$	A_1	2937	2932.2	2926.1	2926.2	0.1	-1.5	-2.2
ν_{19}	νC–H $_{sym}$	B_2						-1.4	-5.1
					2843.0				
					2787.2				
$\nu_{22}+\nu_5$			2576		2569.0				
$\nu_{21}+\nu_{23}$			2256		2247.7				
$\nu_{21}+\nu_7$			2140		2139.7				
					2105.2				
$2\nu_{23}$				1768.3	1778.0	1780.2	2.2		
$\nu_{22}+\nu_{24}$ FR[b]				1747.2	1748.1	1750.5	2.4		
ν_3 FR[b]	νC=O	A_1	1731	1721.4	1725.6	1723.4	-2.2	-1.0	0.5
					1476.2				
ν_{14}	$\delta CH_{3\ as}$	B_1	1454	1451.7	1451.0			3.0	6.5
				1444.3	1441.4	1441.5	0.1		
ν_4	$\delta CH_{3\ as}$	A_1	1435	1429.4	1431.3	1434.1	2.8	0.9	3.4
ν_{20}	δCH_3	B_2	1410	1406.9	1412.3	1415.2	2.9	-2.7	0.9
ν_{21}	$\delta CH_{3\ sym}$	B_2	1363.5	1361.6	1361.1	1361.9	0.8	1.2	2.9
ν_5	$\delta CH_{3\ sym}$	A_1		1354.1	1354.6	1353.3	-1.3	-2.4	1.8
ν_{22}	νC-C $_{as}$	B_2	1215.5	1216.6	1217.4	1222.7	5.3	6.1	3.7
					1191.4				
ν_{15}	rock $CH_{3\ oop}$	B_1	1090.5	1091.7	1090.2	1092.2	2.0	1.7	2.2
ν_{23}	rock $CH_{3\ ip}$	B_2	891	882.4	889			8.0	8.2
ν_7	νC–C $_{sym}$	A_1	777	780.9	782			0.0	2.2
ν_{24}	δC=O $_{ip}$	B_2	530	528.9	528.9	530.2	1.3	1.7	3.1

[a] Wavenumbers in cm^{-1}.

[b] FR, Fermi resonance

[c] ν, stretching; δ, deformation or bend; rock, rocking; sym, symmetric; as, antisymmetric; ip, in-plane; oop, out-of-plane;

4.4 Experimental dimerization enthalpy

The experimental dimerization enthalpy was measured using a van't Hoff plot, illustrated in Figure 6. The underlying equation establishes a linear relation between the inverse temperature and the logarithm of the intensity product $I_{di}/{I_{mon}}^2$, with a slope equal to $-[\Delta H°(LKr) + Rb]/R$ and b being a correction factor to account for the changes in solvent density upon temperature variation.[29] Data sets of acetone solutions in liquid Kr were recorded at temperatures between 134 and 142 K. After resolving the spectra with the least-squares approaches, it was possible to integrate the intensity of a monomer band, I_{mono}, and of the related dimer feature, I_{di}. Figure 6 shows the van 't Hoff plots for two spectral regions, 1860-1640 and 1260-1148 cm^{-1}, that respectively result in complexation enthalpies of -10.3 ± 1.6 and -11.4 ± 1.6 kJ mol^{-1} with error margins equal to twice the standard deviation. The average value, -10.8 ± 1.1 kJ mol^{-1}, compares well with the earlier values of -13.5 ± 1.4 kJ mol^{-1} and -11.7 kJ mol^{-1} reported by Frurip *et al.* [3] and Lin *et al.* [2], respectively, and is line with typical values obtained for other hydrogen and or halogen bonded complexes observed in cryosolutions.[14,19,22,26,50-51] The value is significantly larger than the value of -4.6 kJ mol^{-1} derived from ^{17}O NMR chemical shifts and linewidths.[52]

4.5 Ab initio calculated geometries, energies and wavenumber shifts of the acetone dimer

Although a good agreement is found between the experimental complexation enthalpy derived in this study, and the values reported in literature, some remarks must certainly be made. For example, the experiments reported were conducted at temperatures well below room temperature, while all literature values were derived using data obtained at room temperature or at elevated temperatures. In addition, no corrections for solvent effects discriminating between the gas phase experiments and the experiments in LKr and discriminating between the cryosolutions and the more traditional solvents were introduced.

Recent studies involving a variety of hydrogen and halogen bonded complexes have shown that, after taking into account the necessary corrections for solvent effects and thermal contributions, good agreement can be achieved between experimental complexation energies derived from cryosolutions and theoretical data for the isolated complexes using Complete Basis

Set extrapolations and single point CCSD(T) corrections[37]. To further rationalize the data derived from the cryosolutions, also in this study such calculations were initiated.

In Figure 7 the MP2/aug-cc-pVDZ equilibrium geometries for both geometries are shown. The Cartesian coordinates of the monomers and of the complexes are also given in the Supporting Information. Both structures are characterized by a side-by-side configuration, with the carbonyl being aligned in opposite directions. In agreement with literature data, the most stable geometry has a stacked structure in which the planes of the molecules parallel to each other and perpendicular to the plane through both carbonyl groups.[3,7,53-54] The second, less stable, geometry has a planar structure in which both planes are almost coplanar.

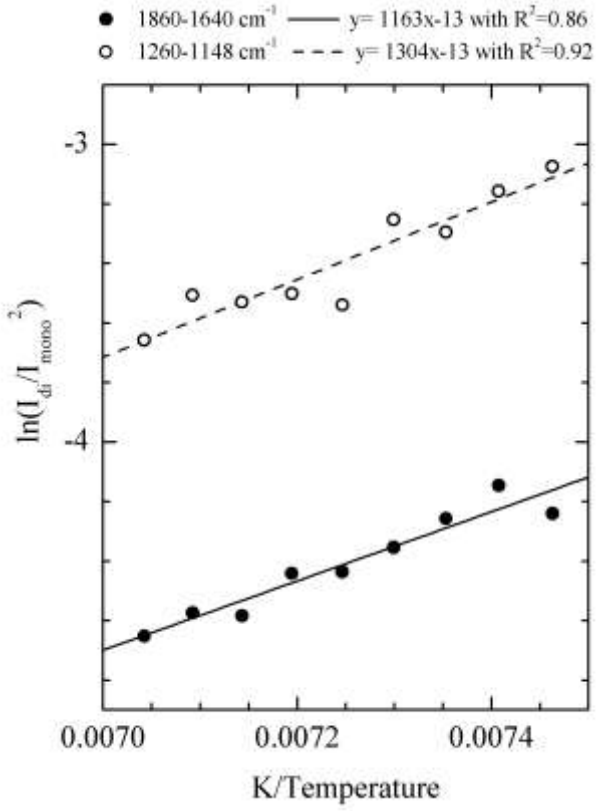

Figure 6. Van 't Hoff plots for the acetone dimer observed in liquid Kr for the spectral region of 1860-1640 (full circles) and 1260-1148 cm^{-1} (open circles) region in the temperature interval 134-142 K.

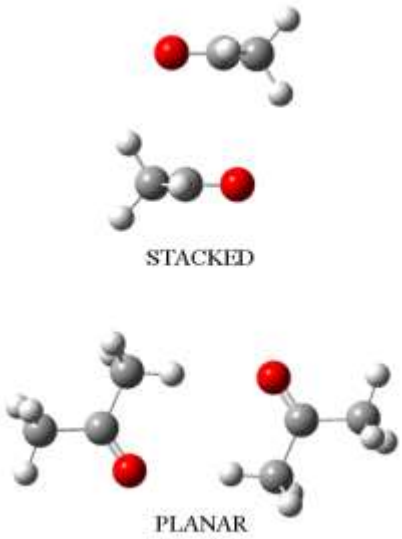

Figure 7. MP2/aug-cc-pVDZ equilibrium geometries for the planar and stacked acetone dimer

It can be noted that the nature of the interaction in the acetone dimers is not always subscribed to dipole-dipole interactions. Hermida-Ramón *et al*.[54] suggested that dimer formation is due to the origination of four C=O···H–C hydrogen bonds, while Frurip *et al* [3] suggested that there are only two of such interactions present. Tamenori *et al*.[9] on the other hand noted that the interaction probably is a combination of dipole-dipole and C=O···H–C hydrogen bonding interactions. Regarding the nature of the interactions between the two acetone units we assume that the long distance (range) dipole-dipole interaction is the driving force for the clustering. But as the distance between the two dipoles shortens a number of C=O···H–C hydrogen bonds arise, creating an extra stabilization to keep the units in the stacked geometry. It should also be mentioned that the actual geometry in the liquid state will not be a rigid antiparallel arrangement of the two dipoles as it will constantly collide with solvent atoms.

Table 2 presents the calculated interaction energies derived from the MP2/aug-cc-pVDZ equilibrium geometries and derived from the and CBS and CCSD(T) single point corrections. To allow comparison with the experimental complexation enthalpies derived from the cryosolutions measurements, the CCSD(T)/CBS based complexation energies ΔE(CCSD(T)) were transformed into vapor phase complexation enthalpies ΔH°(vap,calc), by accounting for thermal and zero-point vibrational contributions. In addition, to estimate the complexation enthalpies in solutions, further noted as ΔH°(LKr,calc), corrections related to the solute-solvent interactions in the

solutions were accounted for. The corrections for zero-point vibrational and thermal influences were based on the standard rigid rotor/harmonic oscillator model regularly used in statistical thermodynamics.[38] The calculations were performed at 138 K for Kr, i.e. at the midpoint of the temperature interval used during the experimental study. The structural parameters and harmonic vibrational frequencies used were obtained by MP2/aug-cc-pVDZ calculations.

The solvent influences on the complexation enthalpies were derived from the solvation Gibbs energies in LKr, obtained by simulating the immersion of monomers and complexes from the gas phase into the solution, using a Monte Carlo Free Energy Perturbation (MC-FEP) approach. To this end, solvation Gibbs energies of monomers and complexes were estimated at 6 different temperatures varying from 127 to 145 K for LKr at a pressure of 28 bar. The enthalpy of solvation $\Delta_{sol}H$ was then extracted using the expressions $\Delta_{sol}H = \Delta_{sol}G + T\Delta_{sol}S$ and $\Delta_{sol}S = -(\partial\, \Delta_{sol}G/\partial T)_p$. Also for these calculations, the MP2/aug-cc-pVDZ equilibrium geometry was used.

Table 2 shows that in agreement with the rather large difference in stability derived for the complexation energies, a significant difference in stability is predicted for the vapor phase complexation enthalpy, the value for the stacked geometry being approximately 8 kJ mol^{-1} more stable than that of the planar geometry.

Table 2 MP2/aug-cc-pVDZ, ΔE(DZ), and the CCSD(T)/CBS,ΔE(CCSD(T)), interaction energies including BSSE corrections, calculated vapor phase interaction enthalpies (vap,calc), calculated interaction enthalpies in LKr (LKr,calc) and corresponding experimentally obtained interaction enthalpies for the planar and stacked acetone dimer (LKr,exp) in kJ mol^{-1}.

	Stacked Dimer	Planar Dimer
ΔE (DZ)	-25.7	-13.0
Δ*E* (CCSD(T))	-28.4	-15.1
ΔH°(vap,calc)	-25.5	-12.1
ΔH°(LKr,calc)	-13.7	-5.8
ΔH° (LKr,exp)	-10.8 ± 1.1	

The large difference in complexation energy suggests that in the cryosolutions studied, the chemical equilibrium is shifted towards complexes with a stacked geometry. Addition information supporting this idea was attempted by comparing the calculated harmonic vibrational wavenumbers for monomers and dimers and by comparing the calculated complexation shifts for planar and stacked geometries with the wavenumber shifts observed experimentally. Although the vibrational spectra of both dimers show only small differences and hence only give rise to small changes in complexation shifts, the linear regression lines give rise to small differences in correlation coefficients, the values being 0.54 for of the stacked dimer and 0.43 for the planar dimer. These results, summarized in Figure S2 of the supplementary information, support the idea stated that the experimental result compares better with the stacked dimer. However, taking into consideration the rather low values for the correlation coefficients obtained, this statement remains tentative.

To account for possible effects of basis sets used and to obtain information on the error margins to be expected for the calculated complexation shifts, calculations were repeated for the the cc-pVTZ and the aug-cc-pVTZ basis sets. The results are included in Figure S2. The results show that for most of the modes considered, the sign of the complexation shifts remains largely unaffected by the choice of the basis set. In contrast, significant changes for the absolute values can be observed for some of the modes. The results further illustrate that for all used basis sets, the correlation coefficients for the linear regression lines are somewhat larger for the stacked geometry. The calculated correlation coefficients for the stacked and planar geometries are 0.54 and 0.43 for the aug-cc-pVDZ basis set, 0.60 and 0.39 for the cc-pVTZ basis set and 0.64 and 0.45 for the aug-cc-pVTZ basis set. The large similarity observed supports the idea that in the cryosolutions, and maybe also in other solutions, the more compact stacked geometry is stabilized. Unfortunately, taking into consideration that for some of the modes the absolute values of the calculated complexation shifts vary significantly, and taking into account that experimental values reported can be influenced for anharmonic effects, solvent effects and thermal effects[21-22], no solid conclusion can be drawn.

5. CONCLUSIONS

Using a data set of spectra of different concentrations at constant temperature, the vibrational spectrum of acetone in liquid Kr was resolved in a monomer and dimer contribution using a newly developed least-squares approach. The assignment of the monomer spectrum fully supports the assignments of the gas-phase spectrum of the compound made by Dellepiane[46]. It was observed that all spectral regions show dimer bands that overlap completely with the related monomer bands except for the dimer band assigned to the $\nu_{C-C\ as}$ mode at 1222.7 cm^{-1} for which a complex band blue shifted from the monomer band by 5.3 $cm^{-1}$is observed. For the first time a complete assignment of the experimental mid infrared spectrum of the acetone dimer was made. Using spectra recorded at different temperatures between 134 and 142 K, the experimental dimerization enthalpy was measured to be 10.8 ± 0.8 kJ mol^{-1}. *Ab initio* calculations predicted a stacked and planar dimer geometry of which the stacked geometry is more stable.

Complexation energies were obtained by combining the MP2 energies and single point corrections involving CCSD(T) calculations and Complete Basis Set extrapolations based on the MP2/aug-cc-pVDZ equilibrium geometry. These calculations lead to complexation energies of -28.4 kJ mol^{-1} for the stacked and -15.1 kJ mol^{-1} for the planar dimer. The corresponding values for the complexation enthalpies in solution, obtained by combining the energies with corrections for thermal and solvent influences are -13.7 and -5.8 kJ mol^{-1}. Additional data supporting the idea that the stacked geometry is strongly preferred in the cryosolutions was attempted by carefully comparing the experimental with theoretical complexation shifts obtained at the MP/aug-cc-pVDZ, MP2/cc-pVTZ and MP2/aug-cc-pVTZ levels. Unfortunately, because of the deviations observed between the values obtained from the different basis sets, and because the experimental values are often influenced by anharmonic, solvent and thermal effects, no unambiguous assignment or a specific geometry could be deduced.

ASSOCIATED CONTENT

Supporting information include info on the numbering of the vibrational modes based on group theory, MP2/aug-cc-pVDZ, MP2/cc-pVTZ and MP2/aug-cc-pVTZ Cartesian coordinates of acetone monomer and acetone dimer geometries, harmonic vibrational frequencies and infrared intensities and complexation energies, and a comparison of experimental and calculated wavenumber shifts.

AUTHOR INFORMATION

Corresponding Author *E-mail: wouter.herrebout@uantwerpen.be. Tel: +32 3 265 33 73.

ACKNOWLEDGMENT

Liene I. De Beuckeleer acknowledges the Research Foundation Flanders, FWO, for the appointment of a PhD Fellowship (11C5814N) and for the financial help towards the purchase of spectroscopic equipment used in this study. The authors thank the Flemish Community for the financial support through the Special Research Fund (BOF). The Hercules foundation and the VSC are thanked for generously providing the required CPU resources. Yannick Geboes is thanked for valuable discussions.

REFERENCES

1. Peter, R.; Dreizler, H., Das Mikrowellenspektrum von Aceton im Torsionsgrundzustand. *Z. Naturforsch. A.* **1965,** *20*, 301-312.
2. Lin, T. F.; Christian, S. D.; Affsprung, H. E., Self-Association and Hydration of Ketones in Carbon Tetrachloride. *J. Phys. Chem.* **1967,** *71*, 968-973.
3. Frurip, D. J.; Curtiss, L. A.; Blander, M., Characterization of Molecular Association in Acetone Vapor. Thermal Conductivity Measurements and Molecular Orbital Calculations. *J. Phys. Chem.* **1978,** *82*, 2555-2561.
4. Tiffon, B.; Ancian, B.; Dubois, J.-E., Natural Abundance ^{17}O NMR as a Tool for Intermolecular Interaction Studies: Acetone Self-Association. *Chem. Phys. Lett.* **1980,** *73*, 89-93.
5. Schindler, W.; Sharko, P. T.; Jonas, J., Raman Study of Pressure Effects on Frequencies and Isotropic Line Shapes in Liquid Acetone. *J. Chem. Phys.* **1982,** *76*, 3493-3496.
6. Knözinger, E.; Wittenbeck, R., Far-Infrared Spectra of Strongly Polar Molecules in Solid Solution: Acetone and Nitromethane. *J. Mol. Spectrosc.* **1984,** *105*, 314-323.
7. Matsuda, Y.; Ohta, K.; Mikami, N.; Fujii, A., Infrared Spectroscopy for Acetone and its Dimer Based on Photoionization Detection with Tunable Coherent Vacuum-Ultraviolet Light. *Chem. Phys. Lett.* **2009,** *471*, 50-53.
8. Guan, J.; Hu, Y.; Xie, M.; Bernstein, E. R., Weak Carbonyl-Methyl Intermolecular Interactions in Acetone Clusters Explored by IR plus VUV Spectroscopy. *Chem. Phys.* **2012,** *405*, 117-123.
9. Tamenori, Y.; Takahashi, O.; Yamashita, K.; Yamaguchi, T.; Okada, K.; Tabayashi, K.; Gejo, T.; Honma, K., Hydrogen Bonding in Acetone Clusters Probed by Near-Edge X-Ray Absorption Fine Structure Spectroscopy in the Carbon and Oxygen K-Edge Regions. *J. Chem. Phys.* **2009,** *131*, 174311.
10. Jalilian, M. R., Spectra and Structure of Binary Azeotropes IV. Acetone-Cyclohexane. *Spectrochim. Acta A* **2008,** *69*, 812-815.

11. Arivazhagan, G.; Elangovan, A.; Shanmugam, R.; Vijayalakshmi, R.; Kannan, P. P., Spectroscopic Studies, NBO Analysis and Dielectric Studies on the Behaviour of Acetone Molecules in Non-Polar Solvent Environment. *Chem. Phys. Lett.* **2015,** *627*, 101-106.
12. van der Veken, B. J.; Delanoye, S. N.; Michielsen, B.; Herrebout, W. A., A Cryospectroscopic Study of the Blue-Shifting C–H···O Bonded Complexes of Pentafluoroethane with Dimethyl Ether-d_6, Acetone-d_6 and Oxirane-d_4. *J. Mol. Struct.* **2010,** *976*, 97-104.
13. Delanoye, S. N.; Herrebout, W. A.; van der Veken, B. J., Stabilities of the C–H···O Bonded Complexes of the Haloforms $HCCl_nF_{3-n}$ (n = 0-3) with Dimethyl Ether, Oxirane, and Acetone: an Experimental and Theoretical Study. *J. Phys. Chem. A* **2005,** *109*, 9836-9843.
14. Hauchecorne, D.; Nagels, N.; van der Veken, B. J.; Herrebout, W. A., C–X···π Halogen and C–H···π Hydrogen Bonding: Interactions of CF_3X (X = Cl, Br, I or H) with Ethene and Propene. *Phys. Chem. Chem. Phys.* **2012,** *14*, 681-690.
15. Herrebout, W. A.; Nagels, N.; van der Veken, B. J., On the $\nu_1^{CO2}/2\nu_2^{CO2}$ Resonance in the Complex of Carbon Dioxide with Dimethyl Ether. *ChemPhysChem* **2009,** *10*, 3054-3060.
16. Geboes, Y.; Proft, F.; Herrebout, W. A., Expanding Lone Pair···π Interactions to Nonaromatic Systems and Nitrogen Bases: Complexes of C_2F_3X (X = F, Cl, Br, I) and TMA-d_9. *J. Phys. Chem. A* **2015,** *119*, 5597-5606.
17. De Beuckeleer, L. I.; Herrebout, W. A., The Self-Associating Behavior of Pyrrole in Liquid Xenon. *J. Mol. Struct.* **2016**, in press.
18. De Beuckeleer, L. I.; Herrebout, W. A., Exploring the Limits of Cryospectroscopy: Least-Squares Based Approaches for Analyzing the Self-Association of HCl. *Spectrochim. Acta A* **2016,** *154*, 89-97.
19. Hauchecorne, D.; Herrebout, W. A., Experimental Characterization of C–X···Y–C (X = Br, I; Y = F, Cl) Halogen-Halogen Bonds. *J. Phys. Chem. A.* **2013,** *117*, 11548-11557.
20. Du, L.; Kjaergaard, H. G., Fourier transform infrared spectroscopy and theoretical study of dimethylamine dimer in the gas phase. *J. Phys. Chem. A* **2011,** *115*, 12097-104.
21. Michielsen, B.; Dom, J. J. J.; van der Veken, B. J.; Hesse, S.; Xue, Z. F.; Suhm, M. A.; Herrebout, W. A., The Complexes of Halothane with Benzene: the Temperature Dependent Direction of the Complexation Shift of the Aliphatic C–H Stretching. *Phys. Chem. Chem. Phys.* **2010,** *12*, 14034-14044.
22. Michielsen, B.; Dom, J. J. J.; van der Veken, B. J.; Hesse, S.; Suhm, M. A.; Herrebout, W. A., Solute-Solvent Interactions in Cryosolutions: a Study of Halothane-Ammonia Complexes. *Phys. Chem. Chem. Phys.* **2012,** *14*, 6469-6478.
23. Michielsen, B.; Verlackt, C.; van der Veken, B. J.; Herrebout, W. A., C–H···X (X=S, P) Hydrogen Bonding: The Complexes of Halothane with Dimethyl Sulfide and Trimethylphosphine. *J. Mol. Struct.* **2012,** *1023*, 90-95.
24. Van Ginderen, P.; Herrebout, W. A.; van der Veken, B. J., van der Waals Complex of Dimethyl Ether with Carbon Dioxide. *J. Phys. Chem. A* **2003,** *107*, 5391-5396.
25. Sluyts, E. J.; van der Veken, B. J., Van der Waals Complexes between Boron Trifluoride and Carbon Monoxide in Liquefied Argon: An Infrared Study. *J. Am. Chem. Soc.* **1996,** *118*, 440-445.
26. Herrebout, W., Infrared and Raman Measurements of Halogen Bonding in Cryogenic Solutions. *Top. Curr. Chem.* **2015,** *358*, 79-154.
27. *MATLAB 8.3*, The MathWorks Inc.: Natick, MA, USA, 2014.

28. van der Veken, B. J.; De Munck, F. R., An Infrared Study of Monomeric and Oligomeric (n=2, 3, and 4) Hydrogen Chloride in Liquified Noble Gases. *J. Chem. Phys.* **1992,** *97*, 3060-3071.
29. van der Veken, B. J., Measurement of Enthalpy Differences in Cryosolutions: Influence of Thermal Expansion. *J. Phys. Chem.* **1996,** *100*, 17436-17438.
30. Delanoye, S. N.; Herrebout, W. A.; van der Veken, B. J., Blue Shifting Hydrogen Bonding in the Complexes of Chlorofluoro Haloforms with Acetone-$d_6$and Oxirane-d_4. *J. Am. Chem. Soc.* **2002,** *124*, 11854-11855.
31. Herrebout, W. A.; Delanoye, S. N.; Maes, B. U.; van der Veken, B. J., Infrared Spectra of the Complexes of Trifluoroethene with Dimethyl Ether, Acetone, and Oxirane: a Cryosolution Study. *J. Phys. Chem. A* **2006,** *110*, 13759-13768.
32. Frisch, M. J.; Trucks, G. W.; Schlegel, H. B.; Scuseria, G. E.; Robb, M. A.; Cheeseman, J. R.; Scalmani, G.; Barone, V.; Mennucci, B.; Petersson, G. A., et al. *Gaussian 09, Revision A.02*, Gaussian, Inc.: Wallingford, CT, USA, 2009.
33. Boys, S. F.; Bernardi, F., The Calculation of Small Molecular Interactions by the Differences of Separate Total Energies. Some Procedures with Reduced Errors. *Mol. Phys.* **1970,** *19*, 553-566.
34. Werner, H.-J.; Knowles, P. J.; Knizia, G.; Manby, F. R.; Schütz, M.; Celani, P.; Korona, T.; Lindh, R.; Mitrushenkov, A.; Rauhut, G., et al. *MOLPRO, version 2012.1, A Package of ab Initio Programs*, 2012.
35. Truhlar, D. G., Basis-Set Extrapolation. *Chem. Phys. Lett.* **1998,** *294*, 45-48.
36. Jurečka, P.; Hobza, P., True Stabilization Energies for the Optimal Planar Hydrogen-Bonded and Stacked Structures of Guanine···Cytosine, Adenine···Thymine, and Their 9- and 1-Methyl Derivatives: Complete Basis Set Calculations at the MP2 and CCSD(T) Levels and Comparison with Experiment *J. Am. Chem. Soc.* **2003,** *125*, 15608-15613.
37. Řezáč, J.; Riley, K. E.; Hobza, P., Benchmark Calculations of Noncovalent Interactions of Halogenated Molecules. *J. Chem. Theory Comput.* **2012,** *8*, 4285-4292.
38. Knox, J. H., *Molecular Thermodynamics*. John Wiley & Sons Ltd: New York, 1971.
39. Jorgensen, W. L., BOSS - Biochemical and Organic Simulation System. In *Encyclopedia of Computational Chemistry*, Schleyer, P. v. R., Ed. John Wiley & Sons Ltd: New York, 1998; Vol. 5, pp 3281-3285.
40. Mellouki, A.; Liévin, J.; Herman, M., The vibrational spectrum of pyrrole (C_4H_5N) and furan (C_4H_4O) in the gas phase. *Chem. Phys.* **2001,** *271*, 239-266.
41. Consani, K., Infrared Bands of Acetone in Solid Argon and the Structure II Clathrate 2Acetylene/Acetone/17Water. *J. Phys. Chem.* **1987,** *91*, 5586-5588.
42. Han, S. W.; Kim, K., Infrared Matrix Isolation Study of Acetone and Methanol in Solid Argon. *J. Phys. Chem.* **1996,** *100*, 17124-17132.
43. Sundararajan, K.; Ramanathan, N., Infrared and *ab Initio* Study of Acetylene–Acetone Complex in Solid Argon and Nitrogen Matrices. *J. Mol. Struct.* **2007,** *833*, 150-160.
44. van der Veken, B. J.; Herrebout, W. A., Conformational Characteristics of Methyl Nitrite: A Cryospectroscopic Study. *J. Phys. Chem. A* **2001,** *105*, 7198-7204.
45. Fishman, A. I.; Herrebout, W. A.; van der Veken, B. J., FTIR Investigation of the Fluorocyclohexane Ring Inversion in Liquid Kr. *J. Phys. Chem. A* **2002,** *106*, 4536-4542.
46. Dellepiane, G.; Overend, J., Vibrational Spectra and Assignment of Acetone, ααα Acetone-d_3 and Acetone-d_6. *Spectrochim. Acta* **1966,** *22*, 593-614.

47. Forel, M. T.; Fouassier, M., Remarques sur le Spectre Infrarouge de l'Acétone et de l'Acétone d_6. *Spectrochim. Acta A* **1967,** *23*, 1977-1980.
48. Mailloux, M.; Weinman, J.; Weinman, S., Fermi Resonance and Intermolecular Forces in ν_{Co} Absorption of Acetone and Acetone-d_6. *C. R. Acad. Sci. C Chim.* **1973,** *276*, 379-382.
49. Cossee, P., Vibrational Analysis of Acetone, Acetaldehyde, and Formaldehyde. *J. Chem. Phys.* **1966,** *44*, 97-111.
50. Geboes, Y.; Nagels, N.; Pinter, B.; De Proft, F.; Herrebout, W. A., Competition of $C(sp^2)$–X···O Halogen Bonding and Lone Pair···π Interactions: Cryospectroscopic Study of the Complexes of C_2F_3X (X = F, Cl, Br, and I) and Dimethyl Ether. *J. Phys. Chem. A* **2015,** *119*, 2502-2516.
51. Nagels, N.; Geboes, Y.; Pinter, B.; De Proft, F.; Herrebout, W. A., Tuning the Halogen/Hydrogen Bond Competition: a Spectroscopic and Conceptual DFT Study of some Model Complexes Involving CHF_2I. *Chem. Eur. J.* **2014,** *20*, 8433-8443.
52. Ancian, B.; Tiffon, B.; Dubois, J.-E., Molecular Interactions and Reorientational Motion of neat Acetone in the Liquid State. ^{17}O NMR Chemical shifts and Linewidths at Variable Temperature. *Chem. Phys.* **1983,** *74*, 171-177.
53. Kollipost, F.; Domanskaya, A. V.; Suhm, M. A., Microscopic Roots of Alcohol-Ketone Demixing: Infrared Spectroscopy of Methanol-Acetone Clusters. *J. Phys. Chem. A* **2015,** *119*, 2225-2232.
54. Hermida-Ramón, J. M.; Ríos, M. A., The Energy of Interaction between Two Acetone Molecules: A Potential Function Constructed from *ab Initio* Data. *J. Phys. Chem. A* **1998,** *102*, 2594-2602.

TABLE OF CONTENTS IMAGE